Plasmon-Mediated Radiative Energy Transfer across a Silver Nanowire Array *via* Resonant Transmission and Subwavelength Imaging

Zhang-Kai Zhou, Min Li, Zhong-Jian Yang, Xiao-Niu Peng, Xiong-Rui Su, Zong-Suo Zhang, Jian-Bo Li, Nam-Chol Kim, Xue-Feng Yu, Li Zhou,* Zhong-Hua Hao, and Qu-Quan Wang*

Department of Physics, Key Laboratory of Acoustic and Photonic Materials and Devices of Ministry of Education, Wuhan University, Wuhan 430072, People's Republic of China

ABSTRACT Efficient plasmon-mediated excitation energy transfer between the CdSe/ZnS semiconductor quantum dots (QDs) across the silver nanowire array up to 560 nm in length is observed. The subwavelength imaging and spectral response of the silver nanowire arrays with near-field point-source excitations are revealed by theoretical simulations. Our studies demonstrate three advantages of the nanosystem: efficient exciton—plasmon conversion at the input side of the array through near-field strong coupling, directional waveguidance and resonant transmission *via* half-wave plasmon modes of the nanowire array, and subwavelength imaging at the output side of the array. These advantages allow a long-range radiative excitation energy transfer with a high efficiency and a good directionality.

KEYWORDS: surface plasmon · silver nanowire array · radiative energy transfer · semiconductor quantum dots · subwavelength imaging

Directional control over the excitation energy transfer between different nanosystems is of critical importance for the emerging field of nanophotonics and has various prospective applications ranging from biological detections to quantum information processing.[1−14] For instance, the excitation energy transfer between semiconductor quantum dots (QDs) is employed to demonstrate quantum operations,[4] and the stimulated interactions between active optical dipoles and surface plasmons are used to generate plasmonic lasing.[5−8] Comparing with nonradiative energy transfer (such as Dexter and Förster processes),[15,16] radiative energy transfer has sufficient distance range but poor efficiency and directionality. The surface plasmons of the exquisitely designing and optimizing metal nanostructures are powerful tools to enhance the efficiency of both radiative and nonradiative energy transfers.[1,17−19] The Ag films have been used by Andrew *et al.* to first demonstrate plasmon-mediated radiative energy transfer from donor to acceptor dye molecules over distances longer than 100 nm,[1] which proceeds in three processes, converting optical dipole of the donors to the surface plasmon on one interface of a Ag film, then cross coupling of two surface plasmons on the opposite interfaces of the film, and finally transferring excitation energy to the acceptors on the opposite side. On the basis of this principle, the corrugated nanostructures have been used by Feng *et al.* to enhance the cross coupling of the two surface plasmons on the opposite interfaces.[17]

A two-dimensional (2D) standing metal nanowire array could be a good candidate to assist radiative energy transfer due to its near-field coupling and imaging behaviors.[20,21] The excitation energy of nanoemitters can be efficiently converted to the surface plasmons through strong coupling near the tips of the Ag nanowires,[10] and the corresponding Purcell factor, P (the ratio of the spontaneous emission rate into the plasmon modes over emission into other channels), is predicted to be as high as 10^3.[22,23] Metal nanorods support both longitudinal and transverse surface plasmon resonances (abbreviated by LSPRs and TSPRs, respectively) by the free electrons near the metal surface oscillating perpendicularly to and along the long axis of the nanorods. Resonant transmission through a Au nanorod array with a far-field excitation is reported by Lyvers *et al.*,[24] which is found to be caused by the half-wave plasmon modes induced by TSPRs in the nanorod array. Furthermore, Ono *et al.* have reported that the metal nanorod array

*Address correspondence to zhouli@whu.edu.cn, qqwang@whu.edu.cn.

Received for review March 21, 2010 and accepted August 17, 2010.

Published online August 25, 2010.
10.1021/nn100578b

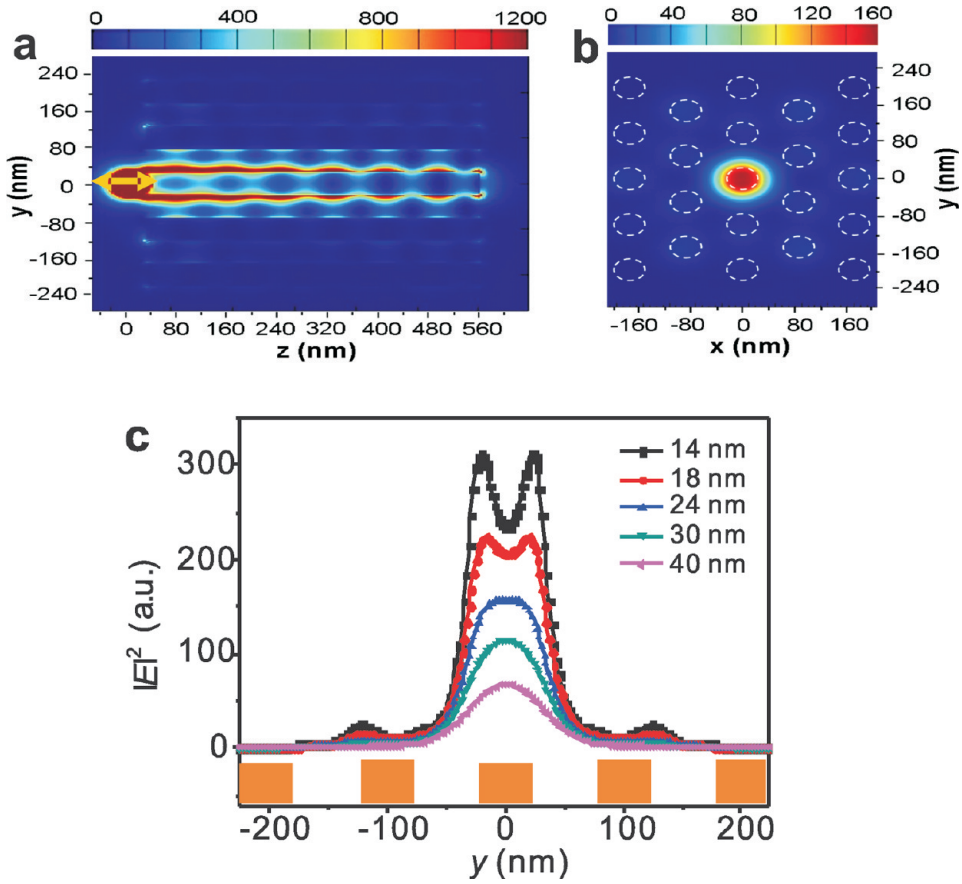

Figure 1. Seventh harmonic half-wave plasmon resonances of the Ag nanowire array (d = 50 nm, a = 100 nm, and L = 540 nm) and the subwavelength imaging of a z-polarized point-source at the center of a nanowire. (a) Field distributions along the nanowires (x = 0, YOZ plane). (b) Subwavelength image at the output plane (z_{out} = 24 nm, XOY plane). The dashed circles represent the positions of the Ag nanowire array. (c) Cross-sectional field distributions at x = 0 and z_{out} = 14, 18, 24, 30, and 40 nm.

has strong near-field focus effects and can generate subwavelength images of a z-polarized nanoemitter at the opposite side of the array when the emission wavelength of the nanoemitter is resonant with LSPRs of the metal nanorods.[20,21] In this paper, we theoretically investigate half-wave plasmon oscillations, resonant transmission, and subwavelength imaging behaviors of the Ag nanowire arrays with near-field point-source excitations and experimentally demonstrate exciton energy transfer between CdSe/ZnS QDs and the corresponding dynamic processes across the nanowire array with length up to 560 nm.

RESULTS AND DISCUSSION

Theoretical Simulations of Subwavelength Imaging by Silver Nanowire Arrays. We begin the studies with computational simulations of the field distributions of a point-source coupling to the surface plasmon of a Ag nanowire array. The simulations are performed by using finite difference time domain (FDTD) method with commercial software FDTD Solutions 6.0.5. In the simulations, the point-source is situated at z = 0 nm and the distance between the point-source and the input side (left end) of the nanowire array is z_{in} = 20 nm (see Figures 1a and 2a), and the 2D hexagonal Ag nanowire array has a period a = 100 nm, wire diameter d = 50 nm. The refractive index of the medium is 1.61.

When a point-source is located at the central axis of a nanowire (as shown in Figure 1), only z-polarized source can be strongly coupled to the nanowire array *via* excitation of LSPRs.[20,25] The propagating field along the nanowires and the output field at the opposite side reach the maxima at one or multiple half-wave resonances of the plasmons (the number of half-wave oscillations is expressed by m). Figure 1a shows the plasmon resonances with m = 7 at λ = 590 nm for the nanowire array with length L = 540 nm (the simulations with m = 1, 2, and 3 are presented in Figure S1 in Supporting Information). The coupled electromagnetic field is mainly confined and propagates near the surface of the central Ag nanowire. It clearly indicates that the electromagnetic field of a point-source strongly couples to and resonantly transmits through the nanowire array *via* half-wave plasmon modes.

After resonant transmission through the nanowire array, the subwavelength images of the point-sources are generated at the output side (right end) of the array due to the near-field imaging effect. Figure 1b

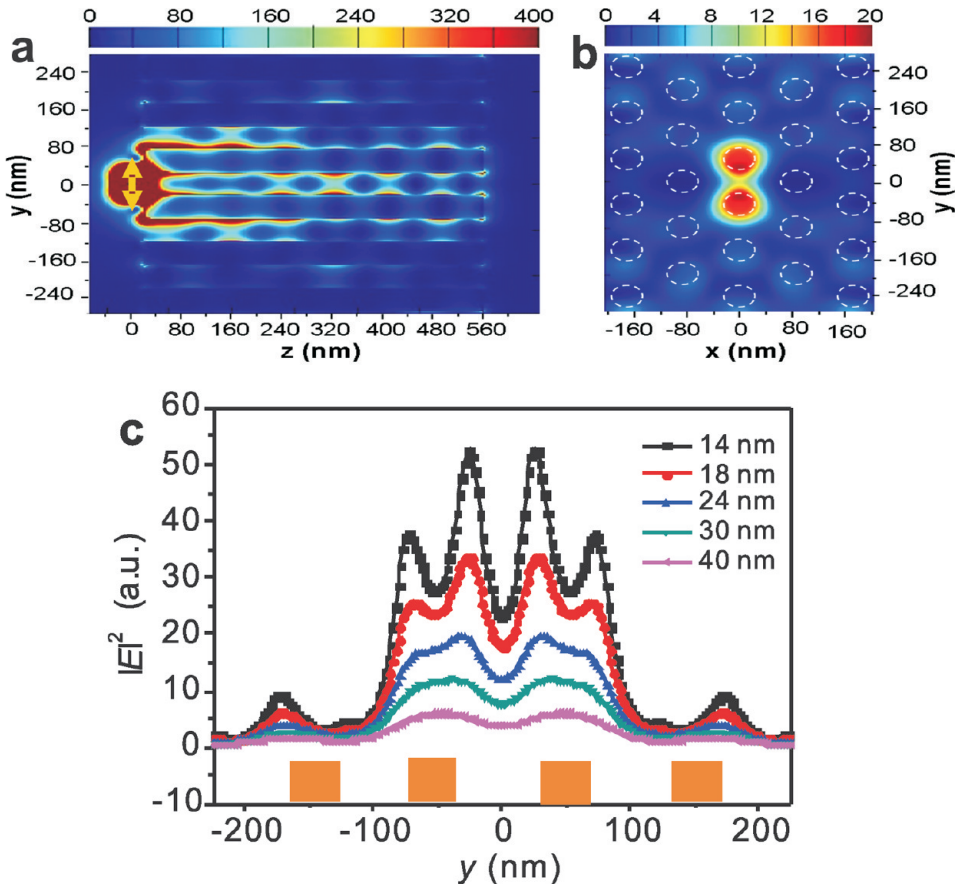

Figure 2. Modulated seventh harmonic half-wave plasmon resonances of the Ag nanowire array (d = 50 nm, a = 100 nm, and L = 540 nm) and two subwavelength images of a y-polarized point-source at the middle of two nanowires. (a) Field distributions along the nanowires (x = 0, YOZ plane). (b) Two subwavelength images at the output plane (z_{out} = 24 nm, XOY plane). The dashed circles represent the positions of the Ag nanowire array. (c) Cross-sectional field distributions at x = 0 and z_{out} = 14, 18, 24, 30, and 40 nm.

shows the subwavelength image at the plane with a distance z_{out} = 24 nm to the output side of the array *via* the seventh half-wave plasmon mode (m = 7). The y cross-section field distributions at x = 0 and z_{out} = 14, 18, 24, 30, and 40 nm are presented in Figure 1c, which demonstrates the formation of the subwavelength image at $z_{out} \approx$ 24 nm, and the full width at half-maximum (fwhm) of the image is as small as 1.4d. Note that the fwhm of the subwavelength image increases from ~70 to ~105 nm when the distance z_{out} increases from 24 to 100 nm (see Figure S3 in Supporting Information).

Interestingly, a y-polarized source is more efficiently coupled to the nanowire array than a z-polarized source when it is located in the middle of two nanowires (see Figure S2 in Supporting Information), and two subwavelength images are generated around two nanowires in this case. Figure 2a shows the modulated half-wave oscillations (m = 7) of a y-polarized near-field source with λ = 590 nm, and the lateral field distribution around a single nanowire is asymmetric due to the transverse plasmons.

Comparing with a single nanowire, the Ag nanowire array has strong lateral near-field interaction between the nanowires as well as large effective lateral cross section, which significantly increases the plasmon coupling to the y-polarized sources (see Figure S4 in Supporting Information). Therefore, the nanowire array generates subwavelength images with much stronger intensity. The collaboration of the longitudinal and transverse plasmons of the nanowire array leads to efficient output of the subwavelength images.

In the spectral domain, the output intensity $|E_{out}|^2$ reaches the maxima (*i.e.*, resonant transmission) when the excitation wavelength of the point-source is resonant with the harmonic half-wave plasmon modes of the Ag nanowire array. The spectral responses of the Ag nanowire array (L = 540 nm) with near-field excitation are shown in Figure 3, where the output field intensities are read out at the plane z_{out} = 24 nm. Three resonant transmission peaks appear near 540, 590, and 650 nm in the visible region, which correspond to the sixth, seventh, and eighth harmonic plasmon resonances, respectively. Note that the spectral responses of the Ag nanowire array for the y-polarized and z-polarized point-sources are only slightly different, which means that the LSPRs of the nanowires play a key role in the half-wave plasmon modes of the array for either y-polarized or z-polarized excitations. We also note

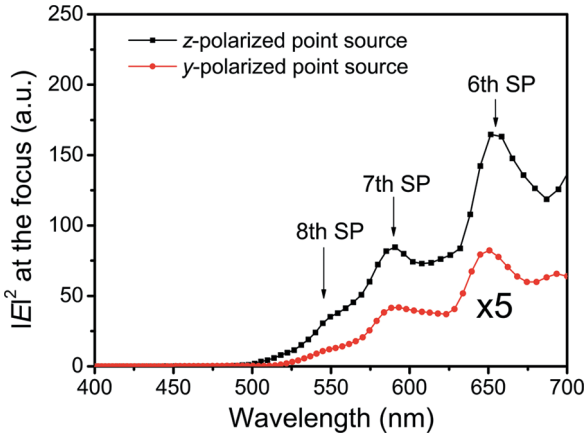

Figure 3. Spectral response in the visible region of the Ag nanowire array (d = 50 nm, a = 100 nm, and L = 540 nm). The point-source is set at the input plane with z_{in} = 20 nm, and the subwavelength imaging intensity is read out at the output plane with z_{out} = 24 nm. Black line: z-polarized point-source at the center of a nanowire. Red line: y-polarized point-source at the middle of two nanowires.

that the short nanowire array with a single half-wave plasmon resonance (m = 1) for z-polarized point-sources corresponds to Ono's superlens.[20] The fwhm value of the subwavelength image of the z-polarized source is almost independent of the value of m, but the longer Ag nanowires (L = 220 nm) supporting the third plasmon mode (m = 3) can focus slightly more energy in the center peak of the near-field images (see Figure S1 in Supporting Information).

The theoretical simulations shown in Figures 1−3 reveal that a point-source (acting as a donor) can be efficiently coupled to the Ag nanowire array, and the subwavelength images can be generated at the opposite side. When an acceptor is located around the subwavelength images of the donor, efficient plasmon-mediated radiative energy transfer from the donor to the acceptor could be expected in this nanosystem.

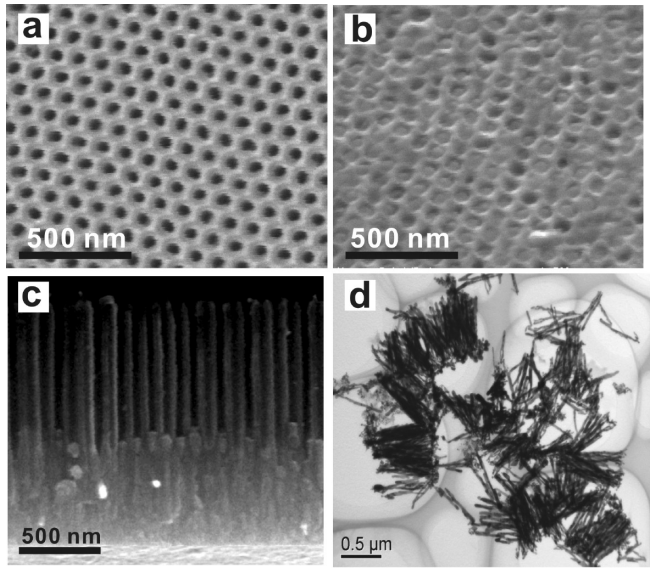

Figure 4. Nanostructures of the Ag nanowire arrays. (a,b) SEM images of the AAO template loaded with the Ag nanowires at the open-pore side and occupied side, respectively. The thin Al_2O_3 barrier layer on the AAO template is removed. (c) Cross-sectional SEM image of the AAO template loaded with Ag nanowires (Q = 300 mC). (d) TEM image of the Ag nanowires (Q = 300 mC). The AAO host medium is dissolved.

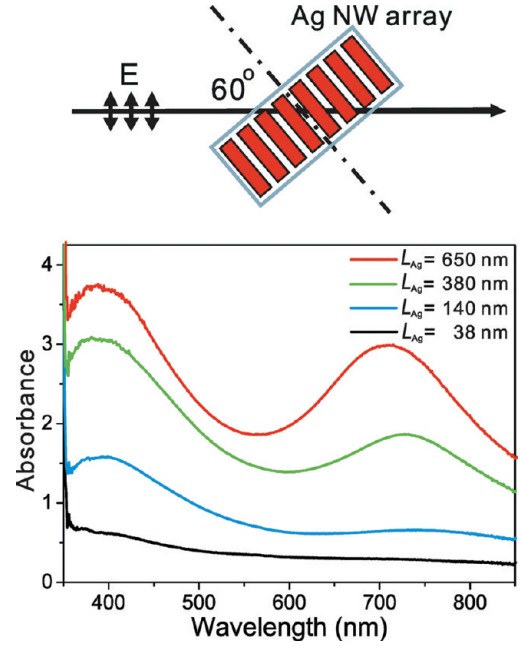

Figure 5. Absorption spectra of the Ag nanowire arrays grown in the AAO templates. The light source is p-polarized and incident with an angle of 60°. The length of the four samples are L_{Ag} = 38, 140, 380, and 650 nm, which are obtained by controlling the electrodeposition charge at Q = 20, 70, 200, and 350 mC, respectively.

Nanostructures and Absorption Spectra of Silver Nanowire Arrays. We turn to experimental demonstrations of long-range excitation energy transfer between QDs by using Ag nanowire arrays, which are electrochemically grown in anodic aluminum oxide (AAO) templates. Figure 4a,b shows the scanning electron microscopy (SEM) images of the AAO templates loaded with the Ag nanowires at the open-pore side and occupied side, respectively. In Figure 4b, the thin Al_2O_3 barrier layer on the AAO template is removed by sputtering technique to uncover the Ag nanowires. A cross-section SEM image of the AAO loaded with the Ag nanowires is shown in Figure 4c. A transmission electron microscopy (TEM) image of the Ag nanowires prepared with electrodeposition charge Q = 300 mC is shown in Figure 4d. From the SEM and TEM images, we estimate that the Ag nanowire arrays have average wire diameter d = 36 ± 3 nm, period a = 97 ± 5 nm, and length L = 560 ± 40 nm.

The absorption spectra of the Ag nanowire arrays with different lengths from 38 to 650 nm (the corresponding electrodeposition charge Q from 20 to 360 mC) are shown in Figure 5. In Figure 5, a p-polarized source with an incident angle 60° is used to excite LSPRs and TSPRs simultaneously. The absorption bands near 400 and 700 nm are caused by TSPRs and LSPRs of the Ag nanowire array, respectively.[26,27] As the average Ag

length increases from ~380 to ~650 nm (the electrodeposition charge Q increases from 200 to 360 mC), the strength of the LSPRs increases about 60%, but the peak position of the LSPRs slightly blue shifts from 727 to 708 nm. This blue shift of LSPRs is mainly caused by the resonances of higher order plasmon modes in the strongly coupled array of Ag nanowires. The similar blue shifts of the LSPRs of the nanowire array were first observed by Evans and co-workers *via* tuning incident angle.[27−29] The transmission behaviors of the Ag nanowire array excited by the far-field and near-field sources are significantly different.

Radiative Energy Transfer between QDs across Silver Nanowire Arrays. The radiative energy transfer is monitored by photoluminescence (PL) emissions. As shown in Figure 6a, an *s*-polarized laser with a wavelength of 400 nm is slantwise (with Brewster angle $\theta_b \approx 50°$) incident to the input sides of the samples, in which the Ag nanowires grow in the AAO template with the donor QDs_D absorbed on the surface of the Al_2O_3 barrier layer and the acceptor QDs_A deposited in the rest of the nanopores of the AAO template. The laser with a short wavelength of 400 nm is blocked by the Ag nanowire array, while the emissions from the donors with a longer wavelength of 560 nm can transmit through the array. Figure 6b shows the PL spectra of the donor-only, acceptor-only, and donor−acceptor samples (all the samples have the same wire length of ~560 nm). For the donor-only sample, the PL (I_D) spectrum shows a peak at ~560 nm, which red shifts about 15 nm compared with that of the dilute QDs_D solution in the absence of Ag nanowire array. This red shift of the PL peak is attributed to the nonradiative Förster energy transfer between the QDs_D in the assembled film and the transmission response of the Ag nanowire array. For the acceptor-only sample, the PL signals (I_A) are not observed in the whole detection region due to the complete block of the direct laser excitations by the Ag nanowire array. For the donor−acceptor sample, a new PL peak at ~660 nm from the acceptor QDs_A is observed, which is attributed to the radiative energy transfer from the donors to the acceptors. If the areas under the donor-only, acceptor-only, and donor−acceptor spectra from 450 to 780 nm are I_D, I_A, and I_{D-A}, respectively, then the energy transfer efficiency is $\eta_{ET} = (I_{D-A} - fI_D - I_A)/I_{D-A}$,[1] where the correction factor f can be calculated from the ratio of the donor emission intensities at 560 nm in the two spectra of donor−acceptor and donor-only samples.[1] From the experimental data shown in Figure 6b, the energy transfer efficiency η_{ET} is calculated to be about 0.7, which means that 70% of the energy transmitted through the Ag array is coupled to the acceptors. Note that the local electric field around the acceptor QDs is enhanced about 2 orders of magnitude in the presence of the Ag nanowire array (see Figure S4 in Supporting Information for details), which indicates that the Ag nanowire

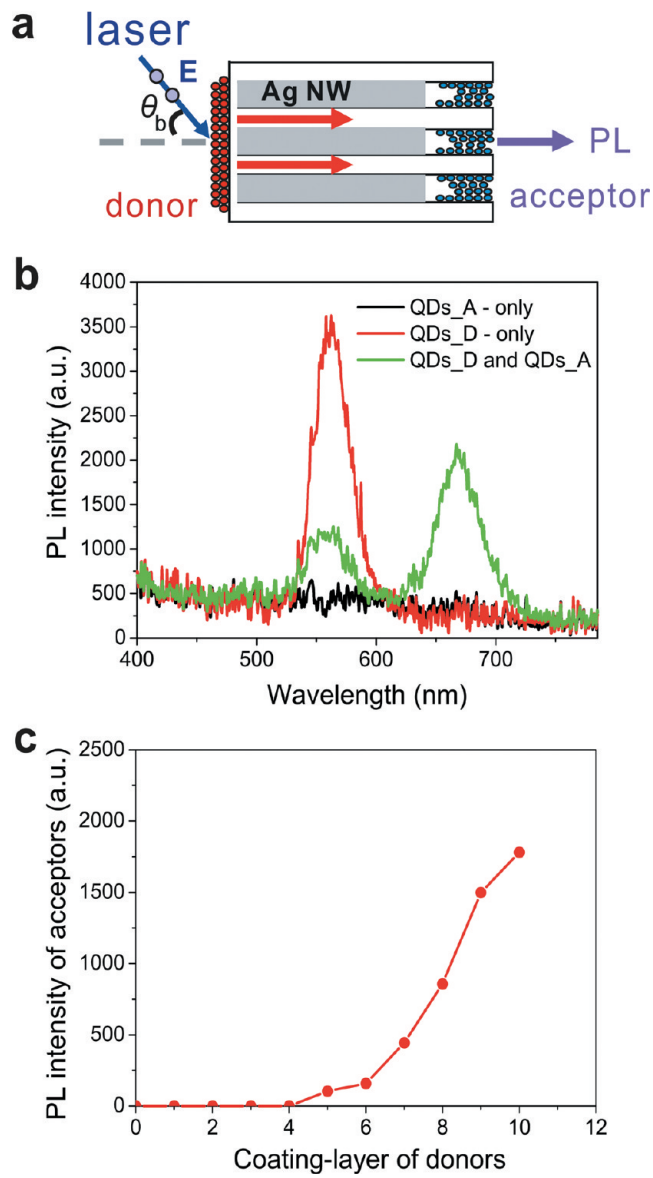

Figure 6. Radiative energy transfer between the QDs across the Ag nanowire array. (a) Illustration of the sample structure with Ag nanowires grown in the AAO template, the donor QDs_D absorbed on the surface of the Al_2O_3 barrier layer, and the acceptor QDs_A deposited in the rest of the nanopores of the AAO template. (b) PL spectra of the donor-only, the acceptor-only, and the donor−acceptor samples. The emissions around 560 and 660 nm are attributed to the QDs_D and QDs_A, respectively. (c) PL intensity of the acceptor QDs_A as a function of the coating layer of the donors absorbed on the Al_2O_3 barrier layer.

array greatly enhances the energy transfer from the donors to the acceptors. The energy transfer efficiency can be further improved by fine-tuning the wire length and decreasing wire length variation.

The PL intensity of the acceptor ($I^{(A)}_{D-A}$) in the donor−acceptor sample has the relationship

$$I^{(A)}_{D-A} \propto N^{(D)}|f^{(D)}(\lambda_{exc})|^2 \frac{\Gamma^{(D)}_{rad}}{\Gamma^{(D)}_{rad} + \Gamma^{(D)}_{nonrad}} T^{(D)}(\lambda^{(D)}_{emi}) N^{(A)} \quad (1)$$

where $N^{(D)}$ and $N^{(A)}$ are the number of the donors and

acceptors, respectively. $\Gamma^{(D)}_{rad}$ and $\Gamma^{(D)}_{nonrad}$ are the radiative and nonradiative decay rate of the donor QDs_D, respectively; $|f^{(D)}(\lambda_{exc})|^2$ is the field enhancement factor of the donors at the excitation wavelength, and $T^{(D)}(\lambda^{(D)}_{emi})$ is the near-field transmittance of the array at the emission wavelength of the donors; $|f^{(D)}(\lambda_{exc} = 400\ nm)|^2$ is calculated by using FDTD method, and the maximal enhancement factor reaches about 8 near the end of the nanowires. The geometry is the same used in Figure 1, but the excitation source is replaced by a 400 nm *s*-polarized plane wave with an incident angle of 50°.

The dependence of the acceptor PL $I^{(A)}_{D-A}$ on the coating layers of the donor films ($n^{(D)}_{Layer}$) is shown in Figure 6c. The value of $I^{(D)}_{D-A}$ is almost zero for the three coating layers of the donor films due to the quenching effect of the Ag nanowire array. This quenching effect can be efficiently depressed by increasing the thickness of the spacer between the QDs_D and the Ag nanowires.[30−33] $I^{(D)}_{D-A}$ dramatically increases when $4 < n^{(D)}_{Layer} < 10$, which is attributed to the coeffects of the large field enhancement factor $f^{(D)}(\lambda_{exc})$ and the strong near-field exciton−plasmon coupling at both excitation and emission wavelengths of the donor QDs_D.

Dynamics of Plasmon-Assisted Radiative Energy Transfer between QDs. The dynamics of exciton−plasmon−exciton−photon conversion and excitation energy transfer are monitored by using a time-correlated single-photon counting (TCSPC) system.[34] The PL decay rate of the donor QDs_D is significantly fastened by the Ag nanowire array, as shown in Figure 7a. The PL decay trace of the QDs on the barrier layer of pure AAO template is single exponential, which means that the cooperative effects caused by the assembling of QDs_D can be neglected. The corresponding PL lifetime is measured to be about 10.7 ns. On the contrary, the PL of 10 coating layers of donor QDs_D transmitted through the Ag nanowire array decays in a two-component exponential form

$$I_{PL}(t) = A_f e^{-t/\tau_f} + A_s e^{-t/\tau_s} \quad (2)$$

where A_f and A_s are the weight factors of the fast and slow decay processes, respectively; τ_f and τ_s are the corresponding lifetimes. By fitting the recorded data, we obtain $\tau_f = 2.2$ ns, $\tau_s = 10.7$ ns, $A_f/(A_f + A_s) = 0.64$, and $A_s/(A_f + A_s) = 0.36$. The enhancement factor of the PL decay rate of the donors reaches as high as 4.9, which confirms a strong near-field coupling between the donors and the Ag nanowire array. The long lifetime contribution is from the donor QDs with longer distance to the nanowires, which are coupled to the plasmons weakly. Figure 7b shows the PL decay rate of the acceptors, which is slightly enhanced by the Ag nanowire array due to the large separation between the acceptors and nanowires because of short deposition time (t_d) (red curve in Figure 7b). As the deposition time is prolonged, the separation decreases, and the emission field of the acceptors is strongly coupled to the nanowires, which leads to a faster PL decay rate of the acceptor QDs_A (black curve in Figure 7b).

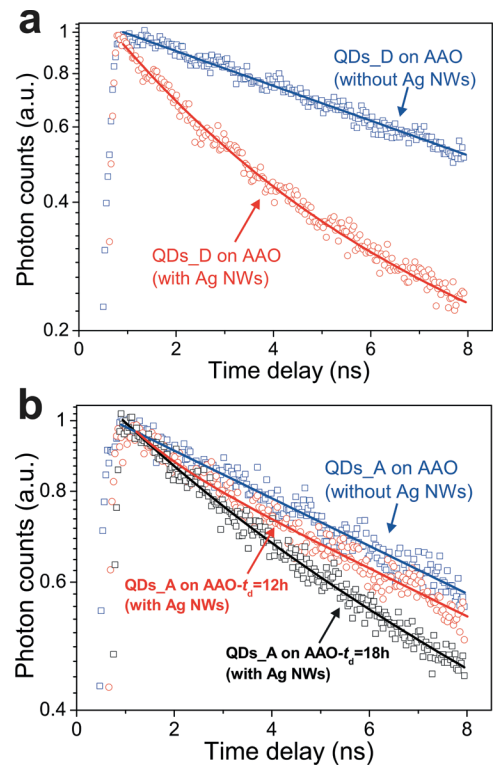

Figure 7. PL dynamics of the donors and acceptors. (a) Normalized time-resolved PL of 10 layers of QDs_D absorbed on the Al_2O_3 barrier layer of the AAO template with and without Ag nanowires. (b) Normalized time-resolved PL of QDs_A deposited in the nanopores of the AAO template with and without Ag nanowires. As the deposition time t_d of QDs_A increases (t_d = 12 and 18 h, respectively, in red and black curves), the separation between QDs_A and Ag nanowires decreases, and the PL decay rate of the QDs_A becomes faster.

CONCLUSIONS

In summary, the Ag nanowire array enhances the excitation energy transfer between QDs by sequential processes: first, enhancing the excitation of excitons in the donors, then converting excitons to surface plasmons through near-field coupling, followed by resonant transmissions of surface plasmons *via* half-wave modes, consequently generating subwavelength images at the opposite side of the array through near-field imaging effect, and finally converting the excitation energy from the images of the donors to the acceptors. The FDTD simulations reveal a more than 10^2 enhancement of the electromagnetic field by the Ag nanowire array over a distance longer than 500 nm. The measured radiative energy transfer efficiency between the QDs reaches about 70% at the output side of the array. The nanowire array demonstrates the conversion of exciton−plasmon−exciton−photon with a higher conversion efficiency compared with single nanowire, and

it assists radiative energy transfer with a longer transmitting distance compared with the Ag film. In addition, the array of longer Ag nanowires also supports multiple half-wave oscillations at multiwavelength and can be used for multicolor subwavelength imaging similarly to the stacked array of the short Ag nanorods (the exquisitely stacked arrangement could be better for color imaging).[21] The metallic nanowire array with half-wave plasmon resonances gives rise to several prospective applications in nanophotonics.

METHODS

Preparation of Samples. The AAO templates were prepared by a two-step anodization process.[34] First, the aluminum sheets (purity 99.999%) were degreased in acetone and electropolished under a constant voltage condition of 16 V for 4 min in a mixture of $HClO_4$ and C_2H_5OH at 0 °C to smooth the surface morphology. In the first and second anodization processes, treated aluminum sheets were exposed to a 0.3 M oxalic acid solution under constant voltage of 40 V in an electrochemical cell at a temperature of about 4 °C. The alumina layer produced by the first anodization process was removed by wet chemical etching in a mixture of phosphoric acid (0.15 M) and chromic acid (0.60 M) at 60 °C for 1 h. The barrier layer of AAO templates was thinned by chemical pore widening and stepwise potential reduced anodization steps.[35] First, the thickness of the barrier layer was decreased by chemically widening in oxalic acid solution at 30 °C for 3 h. Then the AAO templates were anodized with a stepwise reduced potential from 40 V down to 1 V in oxalic acid solution, and the barrier layer was further thinned.

The ordered array Ag nanowires were deposited in the nanopores of AAO templates by pulsed direct current (DC) electrodeposition in an electrolyte containing $AgNO_3$ (0.03 M) and H_2SO_4 acid (0.03 M) with a Pt counter electrode.[36] The deposition pulse was a 6 ms negative potential of −6 V, followed by a 6 ms positive potential of 6 V and a zero potential with delay time of 400 ms. The length of Ag nanowires was controlled by the deposition integral coulomb charge. The deposition was carried on by a galvanostat/potentiostat (PAR VersaSTAT3-200). The underlying Al substrate was dissolved by using $CuCl_2$ solution.

The donor QDs_D were spin-coated and electrostatically absorbed onto the surface of the Al_2O_3 barrier layer of the AAO template layer-by-layer.[37] The freshly cleaned Al_2O_3 barrier layer was functionalized with poly(ethyleneimine) (PEI) to produce a positively charged surface,[38] then a 150 μL droplet of 0.4 μM negatively charged QDs_D solution was dropped on the substrate and rotated for 30 s at 1000 rpm. This procedure was repeated until the needed layers of the QDs_D were achieved. The acceptor QDs_A were deposited into the nanopores at the opposite side of the AAO template loaded with Ag nanowires. Both the donor QDs_D and the acceptor QDs_A are commercial carboxyl CdSe/ZnS core−shell QDs, which were purchased from Invitrogen Corporation. The emission peaks of the QDs are adjusted by their sizes. The donor and acceptor QDs have emission peaks around 545 and 655 nm, respectively.

Characterization of Samples. The filled AAO templates were etched by a precise Ar ion polishing system (Gatan PIPS Model 691) and examined by SEM to determine the degree of pore filling. The SEM was performed by using a FEG SEM Sirion 200 operated at an accelerating voltage of 25.0 kV. The TEM was performed by using a JEOL 2010HT operated at 100 kV. The TEM samples were prepared by dissolving the AAO template containing Ag nanowires in NaOH solution. The absorption spectra were recorded by a UV−vis−NIR spectrophotometer (Varian Cary 5000) by using a *p*-polarized source with an incident angle of 60°.

Optical Experiments. The PL from the samples was collected by the reflection measurement. An *s*-polarized laser for the measurements of PL was generated by a mode lock Ti:sapphire laser (Mira 900, Coherent) with a pulse width of ~3 ps and a repetition rate of 76 MHz. The laser beam was focused into a frequency-double beta barium borate (BBO) crystal, and the excitation wavelength was tuned to ~400 nm, which was near-resonant to the TSPRs of the Ag nanowire array. Therefore, the incident local field at the input side of the nanowire array was enhanced strongly, but the transmission of the excitation laser through the nanowire array was efficiently blocked. The scattering noise was filtered by a band-pass filter (BPF), following by a 70 mm focal length lens, which was used to excite the sample at a Brewster angle $\theta_b \approx 50°$. The luminescence from the sample was collected by the focusing lens and filtered by a couple of filters that consisted of a long wave pass filter (LWPF) and a short wave pass filter (SWPF) before entering the spectrometer detector (Avantes AvaSpec-2048TEC). The time-resolved PL decay traces were recorded by using a time-correlated single-photon counting system (PicoQuant GmbH). The PL measurement precision in our experiments for the samples with multilayered donor QDs reaches about 3% error range due to the high sensitivity of the detector and the strong PL signal from the assembled QDs.

Computational Simulations. The computational simulations were performed by using the FDTD method with perfectly matched layer (PML) boundary conditions. The cell size was $2 \times 2 \times 4$ nm^3. The nanowires were hexagonally arrayed with rod diameter = 50 nm and spacing = 100 nm. The refractive index of the matrix was 1.61, and the complex dielectric constants of the Ag were taken from Palik's handbook.[39]

Acknowledgment. This work was supported in part by NSFC (10534030 and 10874134), National Program on Key Science Research of China (2011CB922201), and Key Project of Ministry of Education of China (708063).

Supporting Information Available: Rod length dependences of the plasmon resonances and subwavelength imaging, excitation−polarization dependences of the plasmon resonances and imaging, output position dependences of the subwavelength image, plasmon coupling efficiency of a dipole to the silver nanowires. This material is available free of charge *via* the Internet at http://pubs.acs.org.

REFERENCES AND NOTES

1. Andrew, P.; Barnes, W. L. Energy Transfer across a Metal Film Mediated by Surface Plasmon Polaritons. *Science* **2004**, *306*, 1002–1005.
2. Andrew, P.; Barnes, W. L. Förster Energy Transfer in an Optical Microcavity. *Science* **2000**, *290*, 785–788.
3. Maier, S. A.; Kik, P. G.; Atwater, H. A.; Meltzer, S.; Harel, E.; Koel, B. E.; Requicha, A. A. G. Local Detection of Electromagnetic Energy Transport below the Diffraction Limit in Metal Nanoparticle Plasmon Waveguides. *Nat. Mater.* **2003**, *2*, 229–232.
4. Lovett, B. W.; Reina, J. H.; Nazir, A.; Briggs, G. A. D. Optical Schemes for Quantum Computation in Quantum Dot Molecules. *Phys. Rev. B* **2003**, *68*, 205319.
5. Bergman, D. J.; Stockman, M. I. Surface Plasmon Amplification by Stimulated Emission of Radiation: Quantum Generation of Coherent Surface Plasmons in Nanosystems. *Phys. Rev. Lett.* **2003**, *90*, 027402.
6. Noginov, M. A.; Zhu, G.; Mayy, M.; Ritzo, B. A.; Noginova, N.; Podolskiy, V. A. Sitimulated Emission of Surface Plasmon Polaritons. *Phys. Rev. Lett.* **2008**, *101*, 226806.
7. Noginov, M. A.; Zhu, G.; Belgrave, A. M.; Bakker, R.; Shalaev, V. M.; Narimanov, E. E.; Stout, S.; Herz, E.; Suteewong, T.; Wiesner, U. Demonstration of a Spaser-Based Nanolaser. *Nature* **2009**, *460*, 1110–1113.
8. Oulton, R. F.; Sorger, V. J.; Zentgraf, T.; Ma, R. M.; Gladden, C.; Dai, L.; Bartal, G.; Zhang, X. Plasmon Lasers at Deep Subwavelength Scale. *Nature* **2009**, *461*, 629–632.

9. Fang, Y. R.; Wei, H.; Hao, F.; Nordlander, P.; Xu, H. X. Remote-Excitation Surface-Enhanced Raman Scattering Using Propagating Ag Nanowire Plasmons. *Nano Lett.* **2009**, *9*, 2049–2053.
10. Wei, W.; Li, S. Z.; Qin, L. D.; Xue, C.; Millstone, J. E.; Xu, X. Y.; Schatz, G. C.; Mirkin, C. A. Surface Plasmon-Mediated Energy Transfer in Heterogap Au−Ag Nanowires. *Nano Lett.* **2008**, *8*, 3446–3449.
11. Chang, D. E.; Sørensen, A. S.; Hemmer, P. R.; Lukin, M. D. Strong Coupling of Single Emitters to Surface Plasmons. *Phys. Rev B* **2007**, *76*, 035420.
12. Rolon, J. E.; Ulloa, S. E. Förster Energy-Transfer Signatures in Optically Driven Quantum Dot Molecules. *Phys. Rev B* **2009**, *79*, 245309.
13. Wei, H.; Ratchford, D.; Li, X.; Xu, H.; Shih, C. K. Propagating Surface Plasmon Induced Photon Emission from Quantum Dots. *Nano Lett.* **2009**, *9*, 4168–4171.
14. Li, Z.; Hao, F.; Huang, Y.; Fang, Y.; Nordlander, P.; Xu, H. Directional Light Emission from Propagating Surface Plasmons of Silver Nanowires. *Nano Lett.* **2009**, *9*, 4383–4386.
15. Dexter, D. L. A Theory of Sensitized Luminescence in Solids. *J. Chem. Phys.* **1953**, *21*, 836–850.
16. Förster, T. Intermolecular Energy Migration and Fluorescence. *Ann. Phys.* **1948**, *2*, 55–75.
17. Feng, J.; Okamoto, T.; Naraoka, R.; Kawata, S. Enhancement of Surface Plasmon-Mediated Radiative Energy Transfer through a Corrugated Metal Cathode in Organic Light-Emitting Devices. *Appl. Phys. Lett.* **2008**, *93*, 051106.
18. Shimada, T.; Tomita, S.; Hotta, S.; Hayashi, S. J.; Yanagi, H. Photoluminescence from Donor−Acceptor Molecular Systems *via* Long Distance Energy Transfer Mediated by Surface Plasmons. *Jpn. J. Appl. Phys.* **2009**, *48*, 042001.
19. Yang, K. Y.; Choi1, K. C.; Ahn, C. W. Surface Plasmon-Enhanced Energy Transfer in an Organic Light-Emitting Device Structure. *Opt. Express* **2009**, *17*, 11495–11504.
20. Ono, A.; Kato, J. I.; Kawata, S. Subwavelength Optical Imaging through a Metallic Nanorod Array. *Phys. Rev. Lett.* **2005**, *95*, 267407.
21. Kawata, S.; Ono, A.; Verma, P. Subwavelength Colour Imaging with a Metallic Nanolens. *Nat. Photonics* **2008**, *2*, 438–442.
22. Chang, D. E.; Sørensen, A. S.; Demler, E. A.; Lukin, M. D. A Single-Photon Transistor Using Nanoscale Surface Plasmons. *Nat. Phys.* **2007**, *3*, 807–812.
23. Chang, D. E.; Sørensen, A. S.; Hemmer, P. R.; Lukin, M. D. Quantum Optics with Surface Plasmons. *Phys. Rev. Lett.* **2006**, *97*, 053002.
24. Lyvers, D. P.; Moon, J. M.; Kildishev, A. V.; Shalaev, V. M.; Wei, A. Gold Nanorod Arrays as Plasmonic Cavity Resonators. *ACS Nano* **2008**, *2*, 2569–2576.
25. Mohammadi, A.; Sandoghdar, V.; Agio, M. Gold Nanorods and Nanospheroids for Enhancing Spontaneous Emission. *New J. Phys.* **2008**, *10*, 105015.
26. Zong, R. L.; Zhou, J.; Li, Q.; Du, B.; Li, B.; Fu, M.; Qi, X. W.; Li, L. T. Synthesis and Optical Properties of Silver Nanowire Arrays Embedded in Anodic Alumina Membrane. *J. Phys. Chem. B* **2004**, *108*, 16713–16716.
27. Evans, P. R.; Kullock, R.; Hendren, W. R.; Atkinson, R.; Pollard, R. J.; Eng, L. M. Optical Transmission Properties and Electric Field Distribution of Interacting 2D Silver Nanorod Arrays. *Adv. Funct. Mater.* **2008**, *18*, 1075–1079.
28. Evans, P.; Hendren, W. R.; Atkinson, R.; Wurtz, G. A.; Dickson, W.; Zayats, A. V.; Pollard, R. J. Growth and Properties of Gold Nickel Nanorods in Thin Film Alumina. *Nanotechnology* **2006**, *17*, 5746–5753.
29. Pollard, R. J.; Murphy, A.; Hendren, W. R.; Evans, P. R.; Atkinson, R.; Wurtz, G. A.; Zayats, A. V.; Podolskiy, V. A. Optical Nonlocalities and Additional Waves in Epsilon-Near-Zero Metamaterials. *Phys. Rev. Lett.* **2009**, *102*, 127405.
30. Anger, P.; Bharadwaj, P.; Novotny, L. Enhancement and Quenching of Single-Molecule Fluorescence. *Phys. Rev. Lett.* **2006**, *96*, 113002.
31. Schneider, G.; Decher, G.; Nerambourg, N.; Praho, R.; Werts, M. H. V.; Blanchard-Desce, M. Distance-Dependent Fluorescence Quenching on Gold Nanoparticles Ensheathed with Layer-by-Layer Assembled Polyelectrolytes. *Nano Lett.* **2006**, *6*, 530–536.
32. Fedutik, Y.; Temnov, V.; Woggon, U.; Ustinovich, E.; Artemyev, M. Exciton−Plasmon Interaction in a Composite Metal−Insulator−Semiconductor Nanowire System. *J. Am. Chem. Soc.* **2007**, *129*, 14939–14945.
33. Fedutik, Y.; Temnov, V. V.; Schöps, O.; Woggon, U. Exciton−Plasmon−Photon Conversion in Plasmonic Nanostructures. *Phys. Rev. Lett.* **2007**, *99*, 136802.
34. Wang, Q. Q.; Han, J. B.; Guo, D. L.; Xiao, S.; Han, Y. B.; Gong, H. M.; Zou, X. W. Highly Efficient Avalanche Multiphoton Luminescence from Coupled Au Nanowires in the Visible Region. *Nano Lett.* **2007**, *7*, 723–728.
35. Nielsch, K.; Müller, F.; Li, A. P.; Gösele, U. Uniform Nickel Deposition into Ordered Alumina Pores by Pulsed Electrodeposition. *Adv. Mater.* **2000**, *12*, 582–586.
36. Sauer, G.; Brehm, G.; Schneider, S.; Nielsch, K.; Wehrspohn, R. B.; Choi, J.; Hofmeister, H.; Gösele, U. Highly Ordered Monocrystalline Silver Nanowire Arrays. *J. Appl. Phys.* **2002**, *91*, 3243–3247.
37. Zimnitsky, D.; Jiang, C. Y.; Xu, J.; Lin, Z. Q.; Tsukruk, V. V. Substrate- and Time-Dependent Photoluminescence of Quantum Dots inside the Ultrathin Polymer LbL Film. *Langmuir* **2007**, *23*, 4509–4515.
38. Decher, G. Fuzzy Nanoassemblies: Toward Layered Polymeric Multicomposites. *Science* **1997**, *277*, 1232–1237.
39. Palik, E. D. *Handbook of Optical Constants of Solids*; Academic Press: New York, 1985.